International Journal of Pharmaceutics: X 5 (2023) 100146

Contents lists available at ScienceDirect

International Journal of Pharmaceutics: X

journal homepage: www.sciencedirect.com/journal/international-journal-of-pharmaceutics-x

Novel cationic cellulose beads for oral delivery of poorly water-soluble drugs

Fan Xie [a], Jernej Slak [b], Pedro Fardim [b], Guy Van den Mooter [a,*]

[a] Drug Delivery and Disposition, KU Leuven, Department of Pharmaceutical and Pharmacological Sciences, Campus Gasthuisberg ON2, Herestraat 49 b921, 3000 Leuven, Belgium
[b] Bio&Chemical Systems Technology, Reactor Engineering and Safety, Department of Chemical Engineering, KU Leuven, 3000 Leuven, Belgium

ARTICLE INFO

Keywords:
Cationic cellulose beads
Swelling
Poorly water-soluble drugs
Solubility improvement
Supersaturation
Amorphous state

ABSTRACT

Cellulose beads emerge as carriers for poorly water-soluble drugs due to their eco-friendly raw materials and favorable porous structure. However, drug dissolution may be limited by their poor swelling ability and the presence of closed pores caused by shrinkage of the pristine cellulose beads. In this study, novel cellulose beads that can swell in acidic environment were prepared by introducing ethylenediamine (EDA) on dialdehyde cellulose (DAC), thereby addressing the shrinkage and closed pore problem of cellulose beads. The effect of the ratio of EDA on the swelling behavior and amine content of beads was studied. Three model drugs with different physicochemical properties were selected to study the physical state of loaded drugs and their release behavior. According to the results of XRPD and DSC, indomethacin and itraconazole loaded in the beads were amorphous at a drug loading of 20%, but fenofibrate was partially crystalline. Both bead size and the ratio of amine groups influenced the release behavior of the model drugs. The *in vitro* dissolution results showed that the cationic beads greatly improved the solubility and dissolution rate of the drug compared with the crystalline drug. Beads with a small size and high ratio of EDA tend to achieve a better drug dissolution rate and cumulative release percentage. Physical stability studies of the itraconazole-loaded beads were also implemented under four different temperature/humidity conditions for up to two months. The results showed that crystallization only appeared after two months of storage at 40°/75% RH, and the drug maintained a non-crystalline state in the other three storage conditions (0 °C/0 %RH, 0 °C/32 %RH, 25 °C/32 %RH). In conclusion, the novel pH-responsive cationic cellulose beads show great potential as a carrier for improving the rate and extent of dissolution of poorly soluble drugs and maintaining supersaturation.

1. Introduction

The demand for renewable resources is growing, considering the future depletion of non-renewable resources (oil, coal, and natural gas) and environmental pollution caused by petroleum-based polymers (Bhan et al., 2020). Natural polysaccharide polymers have attracted increasing attention of scientists because of their nontoxicity, low cost, good biocompatibility, and biodegradability. Among the many polysaccharide materials, cellulose is the largest organic carbon reservoir, with global production (and decomposition) as high as about 1.5×10^{12} tons per year (Klemm et al., 2005). Cellulose can be found in plants, animals, algae, fungi, and even minerals, but the primary source of cellulose is plant fibers (Seddiqi et al., 2021).

The low productivity and high price of natural cellulose cannot meet the growing demand. Regenerated cellulose materials prepared from natural cellulose through dissolving, shaping, and regeneration processes have higher yields and are relatively cheap, which are also environmentally friendly and recyclable. For example, using printed paper wastes to prepare regenerated cellulose beads (Voon et al., 2016). However, the complex network structure and the close packing of numerous hydrogen bonds make the dissolution of cellulose a difficult process. Currently developed "green" solvents for cellulose include ionic

Abbreviations: NASDs, Amorphous solid dispersions; AC, Acetone; CBs, Cellulose beads; DAC, Dialdehyde cellulose; DCM, Dichloromethane; DMSO, Dimethyl sulfoxide; EDA, Ethylenediamine; EtOH, Ethanol; FTIR, Fourier-transform infrared spectroscopy; FNB, Fenofibrate; Tg, Glass transition temperature; HPLC, High performance liquid chromatography; ILs, Ionic liquids; IND, Indomethacin; ITZ, Itraconazole; MeOH, Methanol; mDSC, Modulated differential scanning calorimetry; NCEs, New Chemical Entities; NMMO, *N*-methylmorpholine N –oxide; SGF, Simulated gastric fluid; TBA, Tert-butanol; XRPD, X-ray powder diffraction.

* Corresponding author.
E-mail address: guy.vandenmooter@kuleuven.be (G. Van den Mooter).

https://doi.org/10.1016/j.ijpx.2022.100146
Received 12 December 2022; Accepted 14 December 2022
Available online 16 December 2022

liquids (ILs), sodium hydroxide/urea, NMMO (*N*-methylmorpholine N -oxide)-water system, *etc.*, making the dissolution of cellulose possible and is more environmentally friendly than the solvents used in traditional viscose processes (Jiang et al., 2012; Rosenau et al., 2002; Zhang et al., 2010). By changing the regeneration parameters, different shapes can be obtained according to the application, such as powder, fiber, film, hydrogel, sphere, *etc.* (Fink et al., 2001; Orelma et al., 2020; Wang et al., 2016). Among them, regenerated cellulose beads have a porous structure, high specific surface area, good hydrophilicity, and are often used as adsorbent materials for pollutant treatment (Zhou et al., 2004), chromatographic column stationary phases (Luo and Zhang, 2010), and drug carriers (Voon et al., 2017). Regenerated cellulose beads can be prepared by the dropping method (simple dropping, jet cutting, or electrostatic dropping *etc.*), emulsification (Druel et al., 2020), or more precise processes, such as microfluidics, have also recently been introduced to make cellulose beads, although difficult to scale (Gericke et al., 2013).

Similar to mesoporous silica, the excellent properties of regenerated cellulose beads are believed to be useful as amorphous solid dispersion (ASD) carriers for poorly soluble drugs. However, few articles have reported the successful development of poorly water-soluble drug carriers based on regenerated cellulose beads. Before exploring the reason, it is necessary to understand poorly soluble drugs and amorphous solid dispersions first. Solubility is a key factor in improving oral drug bioavailability, but today, the drug discovery pipeline generates up to 90% of new chemical entities (NCEs) that are inherently poorly soluble and poorly bioavailable (Malamatari et al., 2016). ASD is one of the strategies to improve the water solubility of drugs, the core of which is to convert crystalline drugs into amorphous forms with higher free energy and the use of suitable carriers to increase their stability. Mesoporous materials are ideal carriers because their limited pore size (2–50 nm) can confine the drug molecules into an amorphous or microcrystalline state, effectively preventing the occurrence of recrystallization (Van Speybroeck et al., 2009). Due to the presence of non-ordered drugs, higher dissolution rates and cumulative release are often observed in *in vitro* dissolution experiments, which are favorable signals for improved bioavailability *in vivo*. Voon et al. prepared regenerated cellulose beads of different sizes and investigated their loading and release behavior for curcumin. The dissolution rate decreased with increasing size, and its release curve fits a first-order equation, which was mainly attributed to the Fickian diffusion process of the swollen CB. However, it is worth noting that it takes at least 10 h for the drug loaded in the microbeads to be fully released, even with the smallest particle size (Voon et al., 2017). The same release behavior was reported by Yildir et al., where the dissolution rate of the drug loaded in the beads slowed down as the water solubility of the model drug decreased, even lower than that of the crystalline drug (Yildir et al., 2013). The same results were observed in our previous experiments based on cellulose beads without any modification. Although an amorphous arrangement of the drug was observed from XRPD and DSC results, the release of model drugs from cellulose beads was always extremely low and even lower than crystalline drugs. Possible explanations for the poor release behavior from cellulose beads could be: (1) during the drying process after drug loading, the pores on the surface of the beads are closed or collapsed, thereby reducing the dissolution rate and amount, (2) the swelling ability of the beads in aqueous environment is too low to allow the drug loaded in the beads to be completely released within a certain period of time, and (3) the drug crystallizes on the outer surface of the beads.

From this point of view, functionalization of cellulose can be a solution to solve the existing problems. In our previous study, we used sodium periodate based oxidation to prepare dialdehyde cellulose beads that are soluble in neutral environment (Xie et al., 2022). The introduction of dialdehyde effectively weakened the hydrogen bonding force between cellulose chains, thereby reducing the shrinkage of the beads during drying and drug loading. In addition, the dialdehyde cellulose beads converted the weakly basic model drug to an amorphous form and showed higher supersaturated solutions than the crystalline drug in *in vitro* dissolution experiments. With the dissolution of dialdehyde cellulose in a neutral solution (pH = 7.0), the drug encapsulated inside the beads was continuously released, and the dissolved dialdehyde cellulose was beneficial to the maintenance of drug supersaturation. However, since dialdehyde cellulose does not exhibit swelling properties in acidic solutions, it is less suitable for weakly acidic and neutral poorly soluble drugs. Thus, we hypothesize to further increase the swelling ability of cellulose in acidic solutions by introducing cationic groups. When selecting an amine-containing compound for access, biocompatibility should be considered first, and an amine-containing compound with low toxicity should be chosen. In addition, cross-linking with more hydrophobic compounds such as long-chain and aromatic diamines may reduce the hydrophilicity of cellulose, which is not conducive to drug release. Some simple short-chain diamines, such as ethylenediamine (EDA) are potentially ideal introductions due to their low toxicity and suitable hydrophobicity.

In this study, we introduced different ratios of EDA into dialdehyde cellulose *via* Schiff base reaction and measured its amine group content and swelling ability in different pH environments. Next, three APIs with different physicochemical properties, indomethacin (IND, weakly acidic), fenofibrate (FNB, neutral), and itraconazole (ITZ, weakly basic), were used as model drugs to study the effect of different cation ratios and bead size on drug loading and drug release behavior. The solubilization and supersaturation maintenance effects of cationic beads on the poorly soluble drugs were evaluated.

2. Materials and methods

2.1. Materials

Dissolving pulp from birch wood, obtained from Stora Enso (Helsinki, Finland), was used as a cellulose source, and pretreated as described earlier (De Wever et al., 2021). Sodium hydroxide (97%), urea (≥99.5%), nitric acid (69%), sodium meta-periodate (≥99.0%), and Polysorbate 80 were purchased from Millipore Sigma™ (Darmstadt, Germany). Glacial acetic acid (99%), and NaCl (99.8%) were purchased from CHEM-LAB (Zedelgem, Belgium). Ethylenediamine monohydrate (for synthesis) was purchased from Sigma-Aldrich (Darmstadt, Germany). Hydrochloric acid (36%) was purchased from Fisher Scientific U. K. Limited (Loughborough, UK). Indomethacin (IND), Tert-butanol (TBA,99%) was obtained from ThermoFisher. Fenofibrate (FNB) was purchased from Hangzhou Apichem Technology CO LTD (Hangzhou, China). Itraconazole (ITZ) was procured from Neuland Laboratories Ltd. (Jinnaram, India). Dichloromethane (DCM) and acetonitrile (ACN) were purchased from Fisher Scientific (Loughborough, UK). Methanol (MeOH), Ethanol (EtOH), Dimethyl sulfoxide (DMSO,99.9%) and Ethylene glycol (99.8%) were bought from ACROS Belgium (Geel, Belgium). All solvents were of analytical grade and all materials were used as received.

2.2. Preparation of DAC beads

Cellulose beads (CBs) were prepared following the protocol from Trygg et al. (Trygg et al., 2013). Briefly, 5% pretreated cellulose pulp was dissolved in 7% NaOH/12% urea aqueous solution. The mixture was subsequently cooled to −13 °C while stirring for 2 h until the cellulose pulp was completely dissolved and visually transparent. A syringe pump was used to add the cellulose dropwise into a 2 M nitric acid solution at 25 °C to induce coagulation. After 1 h, the cellulose beads were washed with an excess of deionized water by filtration until the pH of the wastewater is same as deionized water. The beads were stored in deionized water before the oxidation reaction was initiated. Beads of different sizes are prepared by changing the inner diameter of the droplet forming needle. The beads prepared with a 0.8 mm diameter needle were abbreviated as CBs-L, while the beads prepared with a 0.5

Table 1
Added EDA ratio, surface area, pore volume, pore size and amine content of different DAC-EDA samples. -CHO is the aldehyde contents (mmol/g) of DAC4-L and DAC4-S beads.

	Mole ratio of EDA: -CHO	Surface area (m^2/g)	Pore volume (cm^3/g)	Pore size (nm)	-NH_2 content (mmol/g)
Cellulose beads	/	324	1.78	21.5	/
DAC4-EDA0.5-L	0.5:1	163	1.06	26.2	1.41 ± 0.10
DAC4-EDA1-L	1:1	156	1.08	25.7	1.68 ± 0.11
DAC4-EDA1.5-L	1.5:1	129	0.80	24.5	2.06 ± 0.04
DAC4-EDA0.5-S	0.5:1	212	1.43	22.4	1.73 ± 0.22
DAC4-EDA1-S	1:1	178	1.19	25.3	2.01 ± 0.12
DAC4-EDA1.5-S	1.5:1	153	1.00	27.8	2.37 ± 0.02

mm diameter needle were called CBs- S. The beads of both sizes were then oxidized to produce DAC beads. Briefly, 20 g of wet cellulose beads (90% water content) were suspended in 100 mL of deionized water in which 3.3 g of sodium periodate was dissolved. The reaction was carried out at room temperature in the dark (covered the flask with aluminum foil) for 2, 4, 8, 24, 48, and 72 h, respectively. The samples were named according to the oxidation time, for example, a sample oxidized for two hours is denoted as DAC2. The reaction was then quenched by the addition of excess ethylene glycol, followed by repeated washings with deionized water. Specifically, cellulose beads after reaction were immersed in 100 mL deionized water for at least 5 min, then shake the flask fully and pour out the deionized water. Fresh deionized water was added again, and the same process need to be repeated at least 10 times to thoroughly wash away residual solvent.

2.3. Determination of dialdehyde content

The dialdehyde content was determined by the Schiff base reaction between hydroxylamine hydrochloride and the aldehyde group (Dang et al., 2019). Freeze-dried DAC (0.1 g) was grinded to pieces and added to 25 mL distilled water. The pH of the suspension was corrected to 4.50 with 0.1 M HCl. Next, 20 mL Hydroxylamine hydrochloride solution (0.05 g/mL, adjusted to pH 4.50 with 0.1 M HCl) was added to the DAC suspension. The mixture was heated to 40 °C in a water bath for 4 h while gently stirring, and the pH of the solution was finally titrated to 4.50 with NaOH (0.1 mol/L). The -CHO (mmol/g) in DAC was calculated with Eq. (1) by recording the consumed volume of NaOH solution (V_{sample}, mL), while m is the mass of DAC beads. 0.1 g dry cellulose beads were used as a blank, and the consumed volume of NaOH solution was recorded as $V_{control}$ (mL). The tests were run in triplicate.

$$\mathrm{CHO(mmol/g)} = 0.1 \times \left(V_{sample} - V_{control}\right)/m \quad (1)$$

2.4. Amination of DAC beads

10 g of undried DAC4-L and DAC4-S beads (corresponding to 1 g of dry weight) were immersed in 80 mL methanol for solvent exchange, and then DAC, 80 mL of methanol, and different ratios of EDA were added to 100 mL round-bottomed flasks (Table 1). The reaction mixture was kept at 40 °C in a water bath for 2 h, during which time the bottle was shaken every 30 min. After the reaction, the product was repeatedly washed with deionized water and prepared for freeze-drying. The same procedure described in Section 2.2 was used to wash the DAC-EDA beads.

2.5. Determination of amine group content

The content of amine groups in the DAC-EDA beads was evaluated by a titration method (Kim et al., 2017). Briefly, 100 mg dried DAC beads modified with different EDA ratio was immersed into 40 mL deionized water with 10 mL 0.1 N HCl to protonate the free amine. After stirring for 24 h at room temperature, the amount of HCl remaining was determined by titration with 0.1 N NaOH. The -NH_2 (mmol/g) in DAC-EDA was calculated with Eq. (2) by recording the consumed volume of NaOH solution (V_{NaOH}, mL), while m is the mass of DAC-EDA beads, V_{HCl} is the volume of HCl added. The tests were run in triplicate.

$$-\mathrm{NH_2\ (mmol/g)} = 0.1 \times (V_{HCl} - V_{NaOH})/m \quad (2)$$

2.6. Freeze-drying method

A solvent exchange process was used to prepare freeze-dried cellulose beads, during which beads were immersed for at least one hour in consecutive TBA/water mixtures with increasing TBA content ranging from 22.5%, 45%, 67. 5% to 90%. The DAC bead suspensions were flash-frozen using liquid nitrogen and transferred to an ALPHA 1–4 LSC, CHRIST freeze-dryer (Martin Christ Gefriertrocknungsanlagen GmbH). The sample shelf was pre-cooled to −25 °C and kept at constant temperature during the first 36 h of primary drying, then the temperature was increased to −10 °C for another 24 h. The shelf temperature of final drying was 0 °C for 9 h and 10 °C for 3 h, respectively. The following operational conditions were maintained for three consecutive days: the ice condenser was set at −85 °C and the pressure at 0.500 mbar.

2.7. Swelling behavior of DAC-EDA beads

The swelling behavior of freeze-dried DAC-EDA beads in simulated gastric fluid (SGF, pH = 2.0) and phosphate buffer (pH = 7.0) was monitored with an Olympus BX51 polarized light optical microscope (Olympus, Shinjuku, Japan) with an LMPIanFI 10×/0.25 lens (Olympus, Shinjuku, Japan). The microscopic photographs were taken at 0,1,5,10,15, and 20 min, respectively with a TOUPCAM™ digital camera UCMOS03100KPA (ToupTek Photonics, Hangzhou, China) and were displayed *via* ToupView software (version 4.1).

2.8. Drug loading process

The three model drugs were loaded in freeze dried DAC4-EDA beads by the incipient wetness method (Mellaerts et al., 2008). AC and DCM were used to prepare solutions of indomethacin and fenofibrate at a concentration of 40 mg/mL and added dropwise to the beads to obtain a drug loading of 20% *w*/w. The effect of two different solvents on drug physical state and release behavior after loading was investigated. Since the solubility of itraconazole (ITZ) in AC is too low, only dichloromethane was used as the solvent, and the drug loading was also 20% w/w. The loaded beads were dried in a vacuum oven at 25 °C overnight.

The drug load was determined by measuring the difference in weight of DAC beads before and after loading. This was also supplemented by an assay in which beads were immersed in DMSO overnight, after which the concentration of the model drug was quantified using HPLC. The tests were run in triplicate.

2.9. Nitrogen physisorption and calculation

The specific surface area of all freeze-dried DAC beads were quantified by a 3P *meso* 222 sorption analyzer (3P INSTRUMENTS, Odelzhausen, Germany) with N_2 as the sorption gas at −196 °C. All samples were initially degassed at 60 °C for 6 h under vacuum before analysis.

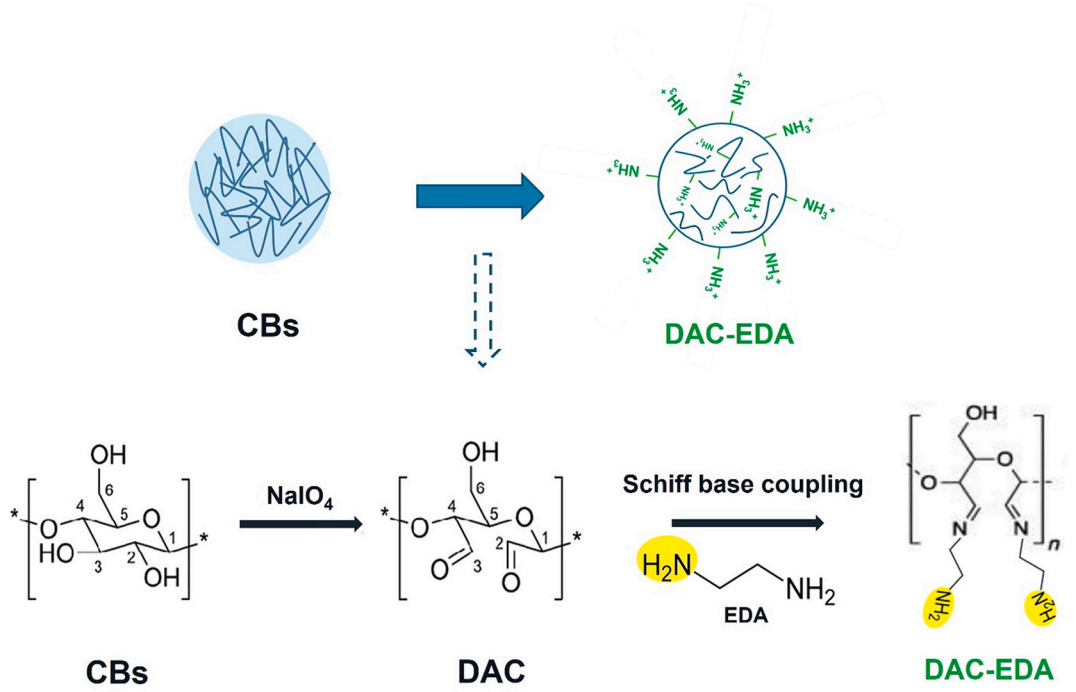

Fig. 1. Scheme of periodate oxidation of cellulose beads and Schiff base reaction with EDA.

The specific surface area was calculated by the Brunauer–Emmett–Teller (BET) method.

2.10. X-ray powder diffraction (XRPD)

XRPD experiments were carried out using an automated X'Pert PRO diffractometer (PANalytical, Almelo, The Netherlands) with a Cu tube (Kα λ = 1.5418 Å) and a generator set at 45 kV and 40 mA. Measurements in transmission mode were performed at room temperature (RT), using Kapton Polyimide thin films (PANalytical, Westborough, MA, USA). A continuous scan mode from 4 to 40° 2θ with a 0.0167° step size and 400 s counting time was applied. X'Pert Data Viewer (Version 1.7, PANalytical, Almelo, The Netherlands) was used to analyze the diffractograms.

2.11. Modulated differential scanning calorimetry (mDSC)

The physical state of model drugs in the beads was investigated with a Q2000 mDSC (TA Instruments, New Castle, DE, USA) using a linear heating rate of 2 °C/min, a period of 40 s and an amplitude of 0.212 °C. Dry nitrogen was used as purge gas at a flow rate of 50 mL/min. Beads were accurately weighed in large standard aluminum DSC pans with volume capacity of 40 μL (TA Instruments, New Castle, DE, USA) and gently pressed with lids to improve thermal contact with the DSC pans. The heating range for IND and ITZ was set from 25 to 180 °C and from −25 to 130 °C in the case of FNB. Universal Analysis 2000 software (TA Instruments, New Castle, DE, USA) was used for data processing.

2.12. Non-sink dissolution testing with pH-shift

The release behavior of the model drugs from DAC-EDA beads was investigated at 37 °C under non-sink conditions using a SR8PLUS dissolution station (SpectraLab Scientific Inc., Markham, ON, Canada) equipped with paddle apparatus II, at a rotation speed of 50 rpm. Each sample was tested in triplicate. More specifically, the release of ITZ from 100 mg DAC-EDA-20%ITZ beads was first performed in 150 mL simulated gastric fluid (SGF, pH 2.0) with 1% polysorbate 80 for 2 h, after which the pH was adjusted to 7.0 by adding 4.0 mL of 0.25 M sodium phosphate solution. The dissolution test was carried out for another 4 h at pH 7.0. Samples were withdrawn at different time points, filtered through a CHROMAFIL® O-45/15 MS PTFE filter (pore size 0.45 μm, MACHERY-NAGEL GmbH & Co. KG, Düren, Germany), and quickly replaced with the same volume of fresh medium. The filtered samples were used to determine the concentration of ITZ by HPLC. Due to the different chemical properties, the dissolution experiments of IND and FNB were performed only in SGF to focus on the solubilization effect of cationic beads on the two model drugs in acidic solution. The drug release behavior in SGF (pH 2.0) containing 0.5% polysorbate 80 for 3 h was measured. The same method was used to extract the samples and determine the drug concentration by HPLC. To compare the effect of cationic cellulose beads, the release profiles of crystalline samples of the three drugs were measured simultaneously.

2.13. Solubility of three model drugs

The solubility of three drugs in different media at room temperature was measured by adding an excess of the model drugs to the medium and continuously stir it for 48 h. Solutions were then centrifuged, the supernatant filtered through a 0.45 μm filter, and the concentration of the drug was quantified using HPLC. All samples were tested in triplicate. For IND and FNB, the test medium was SGF (pH = 2.0) with 0.5% Polysorbate 80. For ITZ, the tested media included SGF with 1% Polysorbate 80 and phosphate buffer with 1% Polysorbate 80.

2.14. HPLC analysis

HPLC-analysis of three drugs was performed using a Merk-Hitachi LaCrom system equipped with a Nucleodur C18 column (150 mm, 4.6 mm ID, particle size 5 μm) obtained from Macherey-Nagel (Düren, Germany). For all samples, the flow rate of the mobile phase was 1 mL/min, and the injection volume of samples was 20 μL. The mobile phase for analysis of FNB consisted of 0.85% (*v*/v) phosphoric acid aqueous solution (pH = 1.5)-ACN (10–90%; v/v), resulting in a retention time of 5 min. For ITZ and IND, the mobile phase consisted of 20 mM sodium acetate buffer (pH 3.5)-ACN (ITZ: 20–80%; v/v, IND: 35–65%; v/v), resulting in a retention time of 3.5 min and 4.5 min respectively. The

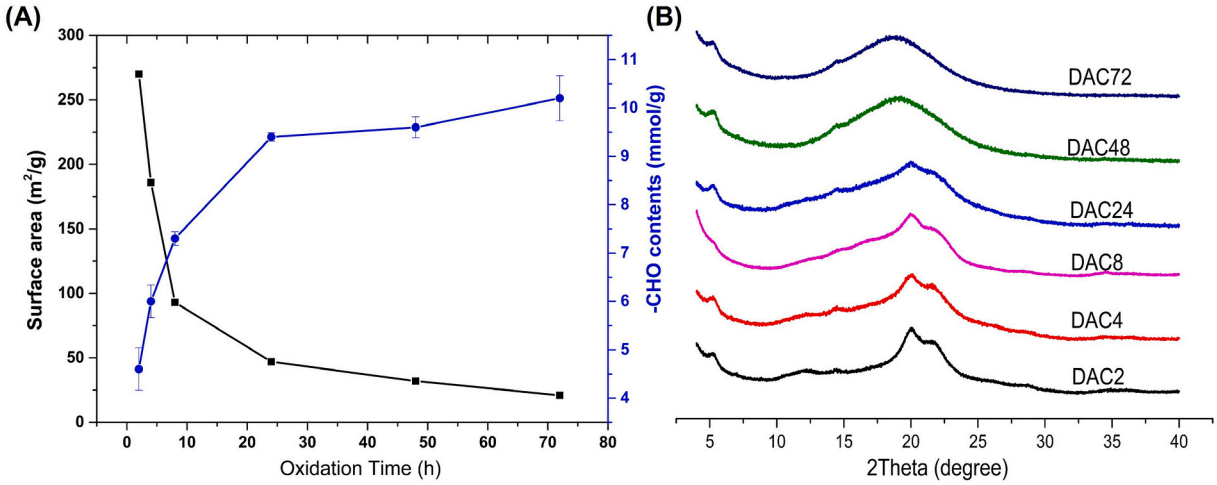

Fig. 2. (A) -CHO content and surface area of DAC-L with different oxidation time. (B) XRPD diffractograms of DAC-L beads with different oxidation time.

methodologies of HPLC were modified from Pas.T et al. (Pas et al., 2018).

2.15. Physical stability study

The stability of the DAC4-EDA1-ITZ was monitored for up to 2 months at four different conditions (0 °C/0 %RH, 0 °C/32 %RH, 25 °C/32 %RH and 40 °C/75 %RH). Periodically (0 days, 14 days, 1 and 2 months) samples were taken and characterized by DSC and XRPD for the presence of crystallinity.

2.16. Statistical analysis of drug release testing

All release experiments were performed in triplicate, and results were expressed as mean ± standard deviation (SD) and indicated as error bars in the release profiles. The final dose percentage or peak percentage of drug from some beads were statistically analyzed using one-way analysis of variance (ANOVA) and Tukey's multiple comparisons test. p values <0.05 were considered statistically significant. Statistical analysis was carried out using Graph Pad Prism 9 software (Graph Pad Software, San Diego, CA).

3. Results and Discussion

3.1. Preparation of DAC-EDA beads

The preparation process of DAC-EDA was carried out in two steps (as shown in Fig. 1): (1) periodate oxidation selectively cleaves the C2-C3 bond of the anhydroglucose ring in the cellulose repeat unit to form two aldehyde groups, (2) one amine group of EDA is bound to the aldehyde group by a Schiff base reaction. To select suitable dialdehyde cellulose for subsequent amine functionalization, beads with different oxidation degrees were prepared by adjusting the periodate oxidation time. The crystal form, specific surface area, pore size, and -CHO content of the samples was characterized. As shown in Fig. 2 (A), with the increase in oxidation time, the -CHO content rapidly increased in the first 24 h, and almost remained unchanged after 24 h. However, a dramatic decrease in the specific surface area was observed with increasing oxidation time. The specific surface area of DAC2 was 270 m^2/g, while that of DAC72 was reduced to only 21 m^2/g. At the same time, the increasing oxidation time also changed the crystallinity of cellulose. From the XRD results (Fig. 2B), DAC2, 4, and 8 showed the characteristic peaks of the cellulose II crystal form. The peak intensity weakened with the increase of the oxidation time, and DAC48 converted to an amorphous structure, showing a broad halo of amorphous cellulose with a maximum at *ca.* 18°(2θ). Considering that the specific surface area is an important determinant for drug loading, and sufficient -CHO content is required to participate in the reaction, we selected DAC4 as the sample for subsequent functionalization.

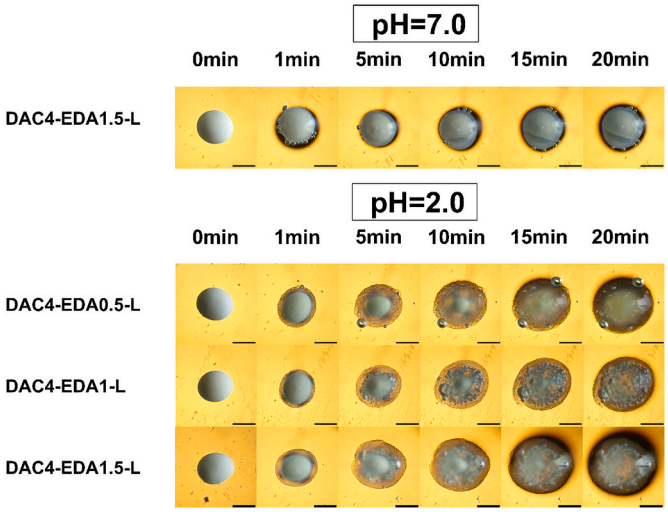

Fig. 3. Optical microscopic images of DAC-EDA0.5-L, DAC-EDA1-L and DAC-EDA1.5-L swelling process in media with different pH. The scale in the figure indicates the length of 1 mm.

According to the aldehyde content of DAC4 (6 mmol/g), different mole ratios of EDA (0.5, 1, and 1.5) were used to prepare DAC4-EDA. The color of DAC4-EDA changed from white to light yellow after functionalization. N_2 adsorption was used to characterize the effect of functionalization on the surface area and pore volume of the beads. The results in Table 1 show that with the increase in EDA ratio, the surface area and pore volume of beads shows a downward trend, but the change in average pore size is negligible. Even so, an average pore size of DAC4-EDA larger than 20 nm is not the best result, as it may produce poor crystallization inhibition effects due to poor confinement effects. For mesoporous systems, smaller pore sizes are required to inhibit nucleation more effectively (Vraníková et al., 2020). The titration results showed that beads with a high EDA ratio had higher amine content, but the amine content of the beads did not increase proportionally to the EDA added. The presumed reason may be that under milder reaction conditions (40 °C), two hours of reaction time is not enough for the complete reaction of amine groups and aldehyde groups. However,

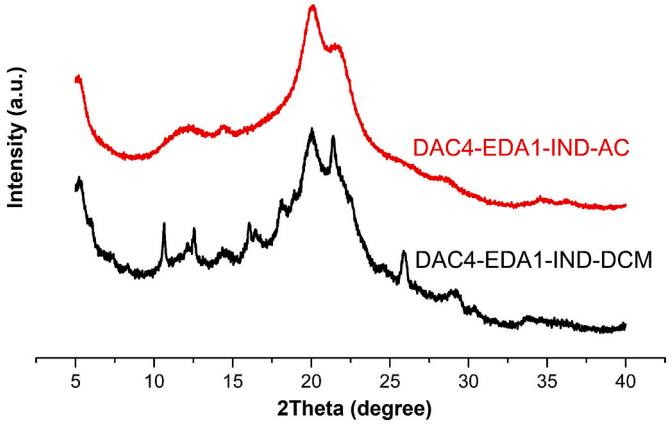

Fig. 4. XRPD diffractograms of DAC4-EDA1-L-IND loaded with AC and DCM.

when we prolong the reaction time, beads with weaker mechanical strength was obtained and difficult to collect resulting in bead breakage and lower yield.

3.2. Swelling ability of DAC-EDA

DAC-EDA was immersed in SGF (at pH = 2.0) and phosphate buffer (at pH = 7.0), and microscopic imaging was performed at different time points to monitor the swelling behavior of the beads. The swelling process of DAC-EDA is shown in Fig. 3. All Beads with different EDA ratios started to swell rapidly after immersion in SGF solution, and a transparent shell could be observed after 1 min. The "core" in the middle of the bead gradually disappeared with the increase of soaking time and completely swelled after 20 min, which was attributed to the electrostatic repulsion between cations in acidic conditions. There was no large difference in the swelling degree of beads with different EDA ratios, but compared with EDA0.5, the swelling rate of EDA1 and EDA1.5 is slightly faster, which can be manifested in a thicker swollen layer at 1 min, and a larger bead size at 20 min. The average diameter of three swollen bead of EDA0.5, EDA1 and EDA1.5 at 20 min was measured to be 2.67 ± 0.11 mm, 2.78 ± 0.17 mm and 3.01 ± 0.15 mm, respectively, which is 1.6, 1.8, and 1.9 times that of the those of their dry beads, respectively.

The swelling behavior of DAC4-EDA1.5 in phosphate buffer (pH 7) was also monitored for comparison. Although a transparent swollen "skin" could be observed after being immersed in the medium, the bead size had only slightly changed, from 1.61 mm to 1.88 mm, while the "core" in the middle still remains after 20 min. The pH-dependent swelling behavior of DAC4-EDA is characteristic of the cationic groups, providing another evidence for the success of the amine group functionalization.

3.3. Characterization of drug loaded DAC-EDA beads

3.3.1. Drug loading solvent

The drugs were loaded into the beads using the incipient wetness method, which means that a high concentration API solution in an organic solvent is added dropwise to the cellulose beads so that the beads absorb the drug solution into the pores by capillarity, thus reducing the possibility of excess solution crystallizing on the bead outer surface and the entrance of the pores. Recently, Dedroog et al. demonstrated that the choice of solvent influenced the phase behavior and physical state of polymer-based amorphous solid dispersions (Dedroog et al., 2021). During the loading process, we also discovered the importance of solvent selection, especially for IND. Since the number of impregnation cycles performed affects the resulting crystallinity of the

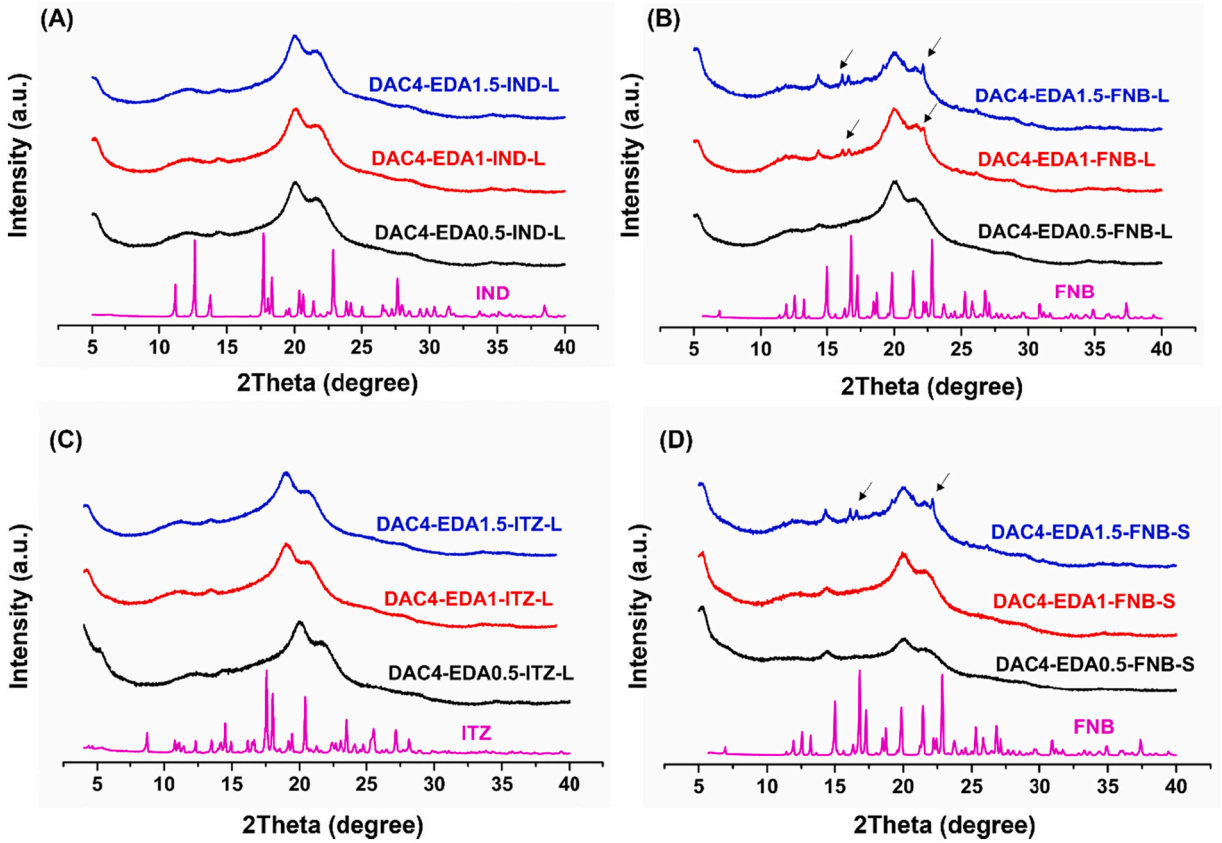

Fig. 5. XRPD diffractograms of (A) DAC4-EDA-IND-L, (B) DAC4-EDA-FNB-L, (C) DAC4-EDA-ITZ-L and (D) DAC4-EDA-FNB-S.

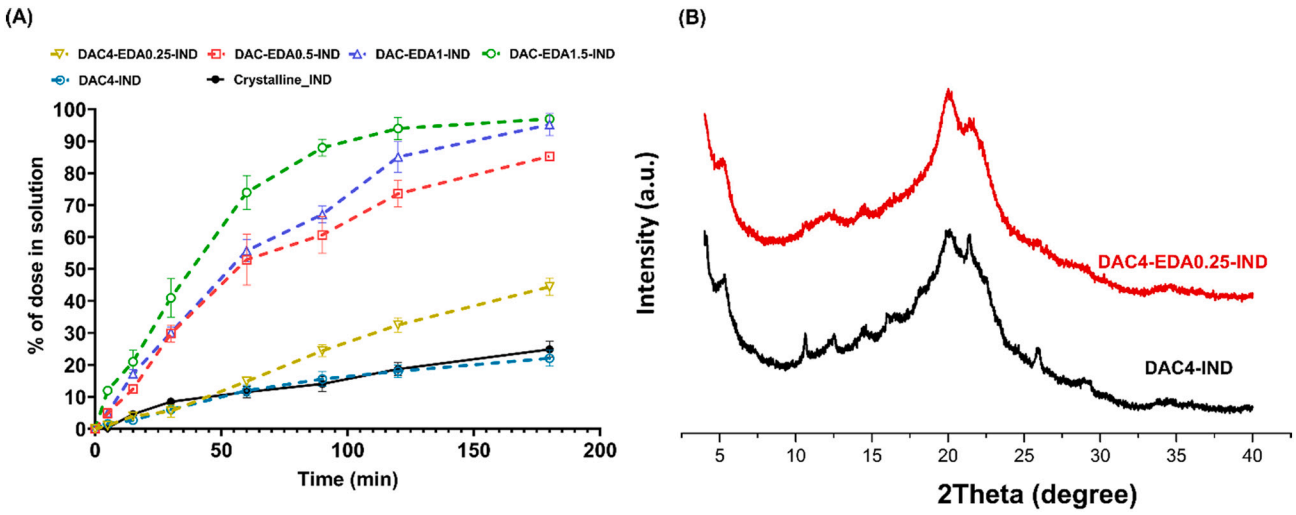

Fig. 6. (A) The release curve of IND from DAC4-L beads with different EDA ratio. (B) XRPD diffractograms of DAC4-IND and DAC4-EDA0.25-IND.

samples, highly concentrated drug solutions are usually used to reduce the number of cycles to obtain higher amorphous drug loadings. In this study, a drug concentration of 40 mg/mL was used. IND had the highest solubility in AC and DCM thus the two solvents were used as candidate solvents.

Taking DAC4-EDA1 as an example, among the samples with the same drug loading of 20%, the samples loaded with DCM as solvent showed the characteristic peaks of crystalline IND in the XRD (Fig. 4), while no Bragg peak can be found in the samples loaded with AC as solvent. The presumed reason is that the solubility of IND in DCM (53.9 mg/mL) is lower than that in AC (65.9 mg/mL). The concentration of the solution used for drug loading was much closer to solubility of IND in DCM. In addition, due to the rapid volatilization rate of DCM, drug deposition may occur before the liquid enters the inner pores, thus causing the formation of crystals on the beads outer surface. The solubility of FNB in both solvents was much higher than 40 mg/mL, so no obvious difference in physical state was found after drug loading. While for ITZ, DCM was chosen as the drug loading solvent due to extremely low solubility in AC (2.5 mg/mL). The solubility of ITZ in DCM was measured to be 239 mg/mL.

3.3.2. XRPD analysis

XRPD was used to characterize the physical state of the three drugs in the DAC-EDA beads (Fig. 5). For IND and ITZ, the drugs showed an amorphous arrangement in all ratios of DAC-EDA-L beads, as Bragg peaks could not be found in the XRPD patterns. The situation was slightly different for FNB, which showed poorer physical stability than the other two drugs due to its lower Tg. Therefore, only beads loaded on DAC-EDA0.5 showed amorphous arrangement, while characteristic peaks of crystalline FNB were found in EDA1 and EDA1.5 samples. The intensity of the peaks increases as the EDA ratio increases, most likely due to the decrease in the specific surface area and/or a change in the pore size of the samples with high ratios of EDA. The DAC-EDA-S sample showed the same XRPD results for IND and ITZ (Fig. S1 A, B), the loaded drug was in an amorphous state. For FNB, DAC4-EDA1 and EDA1.5 still showed characteristic Bragg peaks of crystalline FNB, but the intensity was relatively low compared with DAC-EDA-L. The result can be explained since beads of small size show higher specific surface area for the same mass.

The results obtained by DSC are consistent with XRD, and the total heat flow of IND and ITZ-loaded DAC4-EDA is shown in Fig. S2. In all beads loaded with IND and ITZ, no melting peaks representing crystalline drugs were found, demonstrating a completely amorphous arrangement of drugs. For FNB(Fig. S3A), the melting peak of FNB was found in DAC4-EDA1-L and DAC4-EDA1.5-L samples at around 72–75 °C (indicated by black arrows) in reserving heat flow, proving the existence crystalline FNB (polymorph II) (Tipduangta et al., 2015). The same results were found in small-size DAC4-EDA1.5 beads (Fig. S3B).

Table 2
Comparison of drug release data of the DAC-EDA beads with different EDA ratio and crystalline IND.

	C_{max} (% IND)	t_{max}(min)	AUC (%.min) (x10^3)
Crystalline-IND	24.9 ± 2.5	180	2.61 ± 0.31
DAC4-L	22.1 ± 2.4	180	2.44 ± 0.30
DAC4-EDA0.25-L	44.5 ± 2.8	180	4.16 ± 0.70
DAC4-EDA0.5-L	85.3 ± 0.7	180	10.14 ± 0.56
DAC4-EDA1-L	95.2 ± 3.5	180	11.35 ± 0.64
DAC4-EDA1.5-L	97.0 ± 1.1	180	13.28 ± 0.31

3.4. Non-sink dissolution testing of DAC4-EDA beads

The dissolution profiles of the three model drugs are shown in Fig. 7. The dissolution profile of the crystalline drug substance (black curve) was used as a control. Overall, all beads showed faster dissolution rates and higher cumulative release than the crystalline drugs, achieving solubilization of the poorly soluble drugs. To explain the release more clearly, we focused on analyzing the influence of two important factors on the release behavior, namely the ratio of EDA and the size of the beads.

3.4.1. Effect of EDA ratio on release

We used DAC-EDA-L as a representative to analyze the effect of different ratios of EDA on IND release (Fig. 6A), where the release curves of DAC beads without amine groups (*i.e.*, DAC4) and DAC4-EDA0.25 were also added for comparison. The release curve of IND from DAC4 was almost same as the dissolution profile of crystalline IND, demonstrating that DAC4 beads cannot increase the dissolution rate of IND. The reason is that, firstly, DAC4 has no swelling capacity, thus the drug loaded inside of the beads needs a longer time to contact the medium and dissolve. In addition, the characteristic Bragg peak of IND appears in the XRPD result of the DAC4 sample. The existence of crystalline IND in DAC4 also affects the dissolution rate. Compared with DAC4, the introduction of EDA showed a positive effect on improving the dissolution rate of IND. As shown in Fig. 6(A), beads prepared with a mole ratio of 0.25:1 EDA/-CHO increased the dissolution percentage of IND from 20% to 40% after 3 h of release testing. The dissolution rate of IND increased with the increase of EDA ratio, while the swelling and

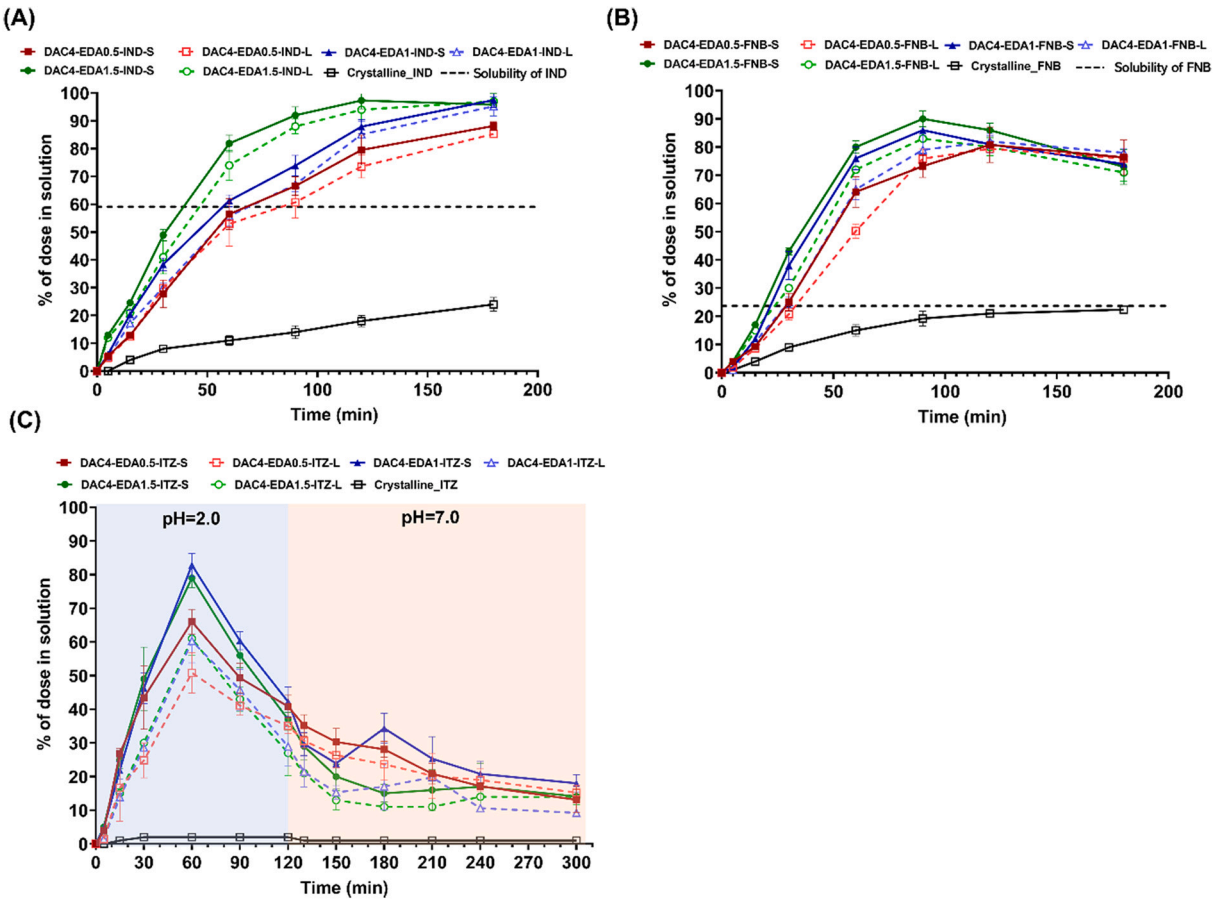

Fig. 7. *In vitro* release curve of three model drugs, (A) IND, (B) FNB and (C) ITZ from different size of DAC4-EDA beads. Black horizontal dashed lines represent the solubility of IND and FNB.

dissolution rates of DAC4-EDA-1 and DAC4-EDA-1.5 were also observed to be faster than EDA0.25 and EDA0.5 during the dissolution process. The final release of IND from DAC4-EDA0.5, DAC4-EDA1 and DAC4-EDA1.5 beads were 85.3 ± 0.7%, 95.2 ± 3.5%, 97.0 ± 1.1%, respectively (Table 1). The area under the curve (AUC) is calculated and shown in theTable 2. DAC4-EDA1.5 has the highest AUC which is 5-fold of crystalline IND. The final dose percentage of DAC4-EDA0.5, DAC4-EDA1 and DAC4-EDA1.5 shows significantly different as compare with crystalline IND ($p < 0.05$). The increase of release from EDA0.25 to EDA0.5 is the largest, while the increment between three high EDA ratio samples becomes smaller. This result demonstrates that the modifiable -CHO on DAC4 becomes limited after 0.5 ratio of EDA, which is consistent with the -NH_2 content measured by titration. At the same time, the XRPD results showed that although a small amount of crystalline IND was still present in DAC4-EDA0.25, its crystallinity decreased compared to DAC4 (Fig. 6B). In general, the introduction of EDA not only increases the dissolution rate and percentage but also increases the ability of the amorphization of IND and showed an upward trend as the proportion of EDA increased.

3.4.2. *Effect of beads size on release*

Smaller beads are expected to have faster dissolution rates because of the increased surface area accessible to the medium. Thus, the *in vitro* release behaviors of the two sizes of beads for the three model drugs were compared, and the results are shown in Fig. 7 (the dashed line is the release curve of large-size beads, and the solid line represents the release of small-size beads). Overall, DAC4-EDA-S always show a higher release than DAC4-EDA-L, although sometimes the difference is not noticeable. For IND, the highest release occurred in the sample DAC4-EDA1.5-S with release percentage of 97.3 ± 2.7%. The DAC4-EDA1.5-S shows the highest AUC among all type of beads, which is 5.3 times that of crystalline IND, and almost complete release was achieved. The lowest AUC was given by sample DAC4-EDA0.5-L, which is still 3.9 times that of the crystalline IND (more details can be found in Table S2). No significantly different ($p > 0.05$) can be observed between -L beads and —S beads on IND dissolution behaviors. The saturated solubility of IND in SGF + 0.5% polysorbate 80 is 59.1% (shown by the black dashed line in Fig. 7A), which proves that the release of IND from all beads reaches a supersaturated state after 90 min and is well maintained for the subsequent 90 min. The dissolution data of FNB from DAC-EDA beads with different size and EDA ratio and crystalline FNB were shown in Table S2. The saturated solubility of FNB in SGF + 0.5% polysorbate 80 was 23.7%, so FNB was almost supersaturated after 30 min of release from all bead samples and continued to rise. DAC4-EDA1.5-S showed the fastest dissolution rate and reached the maximum release at 90 min (90.0 ± 2.8%), followed by DAC4-EDA1-S (86.0 ± 1.0%). However, the drug concentration exceeds the saturation concentration by nearly 4 times at that time, and the risk of drug crystallization increases. A drop in concentration was observed from 120 min and the final release of DAC4-EDA1.5-S decreased to 73.0 ± 6.2%. For beads that show slower drug release, such as DAC4-EDA0.5-L and —S, although a slightly lower percentage of maximal release was achieved (DAC4-EDA0.5-L: 79.4 ± 1.1%, DAC4-EDA0.5-S: 80.8 ± 6.2%), the drop in concentration caused by recrystallization was more slowly, resulting in a final release comparable to DAC4-EDA1.5-S after 3 h. In the case of ITZ, the beads continuously dissolved in SGF + 1% polysorbate 80 to release the encapsulated drug and reached a maximum release after 60 min. Subsequently, due to the instability of the supersaturated solution, crystallization occurs rapidly, resulting in a sharp decrease in drug concentration. The effect of bead size on ITZ

Table 3
Comparison of drug release data of the DAC-EDA beads with different size and crystalline ITZ.

	C_{max} (% ITZ)	t_{max}(min)	AUC (%.min) (x10^3)
Crystalline-ITZ	2.0 ± 1.2	30	0.39 ± 0.06
DAC4-EDA0.5-S	66.0 ± 3.7	60	9.53 ± 1.02
DAC4-EDA0.5-L	50.8 ± 5.9	60	7.98 ± 1.23
DAC4-EDA1-S	82.8 ± 3.5	60	10.80 ± 1.01
DAC4-EDA1-L	60.2 ± 6.2	60	7.15 ± 0.91
DAC4-EDA1.5-S	79.0 ± 2.9	60	9.30 ± 1.25
DAC4-EDA1.5-L	61.0 ± 5.1	60	6.88 ± 0.80

release behavior appears to be more pronounced. All small-size beads showed higher maximum release and faster dissolution rates. The peak concentrations of ITZ when using DAC4-EDA1 and DAC4-EDA1.5 are very close, which are 82.9 ± 3.5% and 79.4 ± 2.9%, respectively (Table 3). The maximum release percentages corresponding to the large-size beads are only 60.2 ± 6.5% and 61.0 ± 5.1%. The difference between -S and -L beads is around 20%. Since ITZ is a weakly basic drug, a decrease in the concentration of crystalline ITZ was observed after adjusting the pH to 7.0. However, all bead samples still maintained at least ten-fold higher concentrations than that of crystalline ITZ. It is worth emphasizing that compared with the extremely low solubility of ITZ, regardless of the type of beads, the beads as a carrier greatly improved the dissolution rate of ITZ in *in vitro* dissolution experiments, which is a great improvement and means that DAC4 -EDA beads also have the potential to enhance the bioavailability of ITZ *in vivo*.

3.5. Physical stability study

ITZ was selected as a model drug to determine the physical stability of DAC4-EDA-loaded ITZ over two months. The results of XRPD and DSC shown in Fig. 8 and Fig. 9 demonstrate the physical state of ITZ at different time points. The XRD results showed that all the samples stored at four different conditions remained in the amorphous state, and no characteristic peaks of crystalline ITZ can be found even after two months of storage (Fig. 8). Different results were found in DSC. No

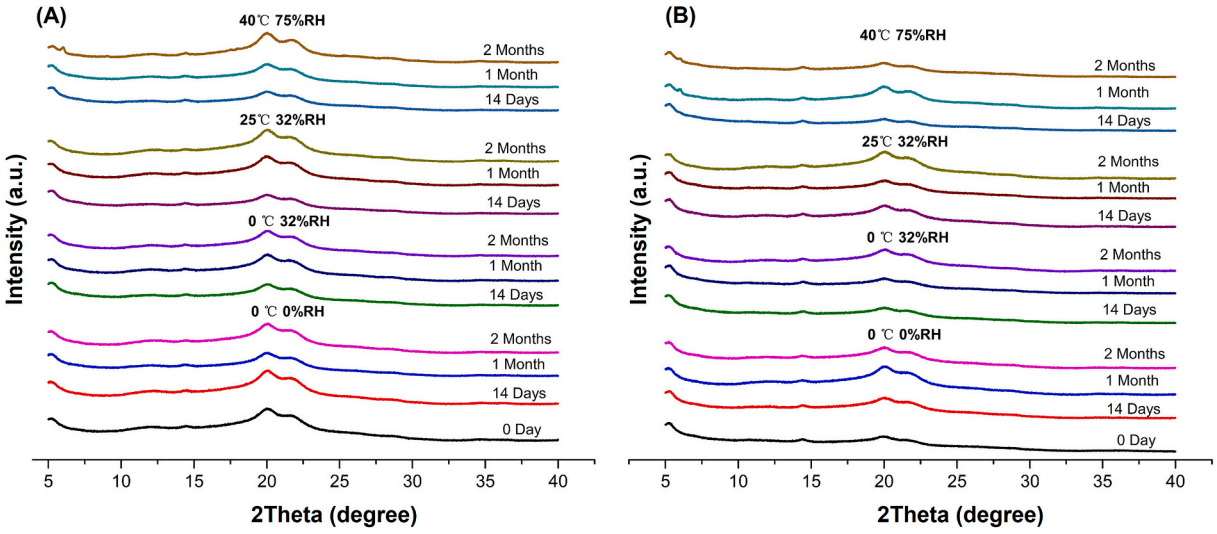

Fig. 8. XRPD diffractograms of (A) DAC4-EDA1-ITZ-S and (B) DAC4-EDA1-ITZ-L stored under different conditions for 14 days, one month and two months.

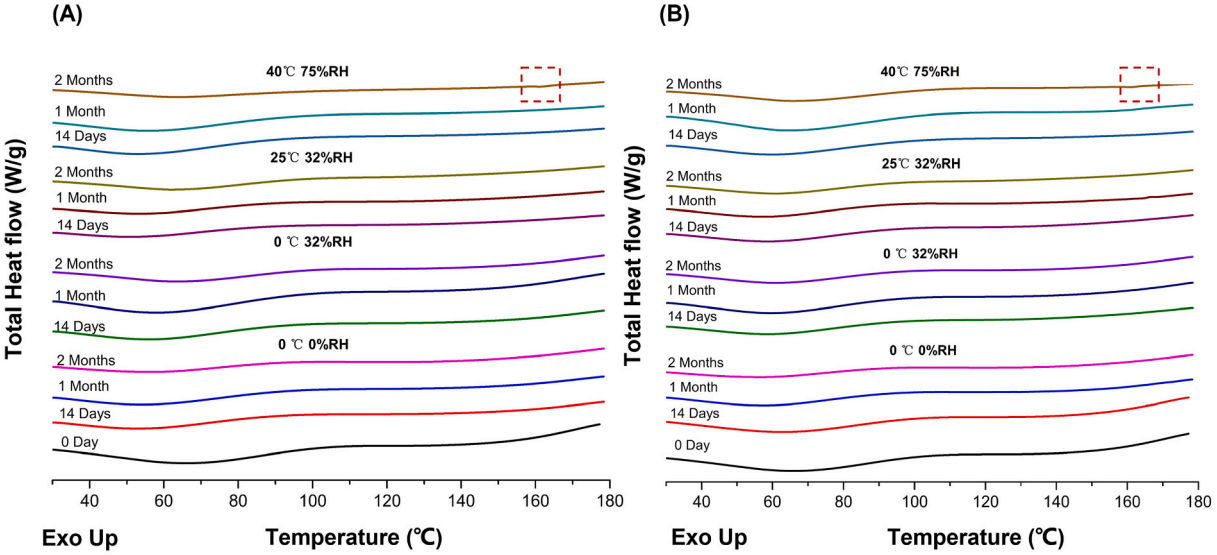

Fig. 9. DSC thermograms of (A) DAC4-EDA1-ITZ-S and (B) DAC4-EDA1-ITZ-L stored under different conditions for 14 days, 1 month and 2 months. Red dashed boxes indicate the melting peaks of ITZ appeared in samples after stored at 40 °C/75 %RH for 2 months. (For interpretation of the references to color in this figure legend, the reader is referred to the web version of this article.)

melting peak of ITZ was detected in DSC after two months of storage at 0 °C/0 %RH, 0 °C/32 %RH and 25 °C/32 %RH, proving that the drug still exists in an amorphous state. However, after two months of storage at 40 °C/75 %RH, a very small melting peak of ITZ at 161.6 °C can be found in both DAC4-EDA1-L and DAC4-EDA1-S samples, as marked by the red dashed box in the Fig. 9. The enlarged DSC result can be found in Fig. S4. The difference in the results is due to the higher sensitivity of DSC than XRPD.

We also noticed a color change of the beads after storage at 25 °C/32 %RH and 40 °C/75 %RH for two months: from pale yellow to dark brown (Fig. S5). Most likely, the dark brown color is the product of the Maillard reaction. DAC chains, containing active carbonyl groups will undergo a carbonyl–amine reaction with the highly reactive primary amine group (Liu et al., 2021; Schuster and Lindner, 2011). The required conditions of this reaction are mild, and no catalyst is required. Since high temperature and humidity are factors that promote the reaction, significant browning of the beads was observed at 25 °C/32%RH and 40 °C/75%RH conditions. The results of the physical stability experiments show that when using amine-functionalized dialdehyde cellulose as a drug carrier, not only the stability of the amorphous drug loaded in the beads, but also the possible changes in the beads should be considered. According to the results, ITZ can maintain its stability for 2 months in the other three conditions except for 40 °C/75 %RH, while the browning of the beads themselves can be effectively inhibited in 0 °C /0 %RH and 0 °C/32 %RH storage conditions. Thus, the ideal storage conditions of DAC4-EDA-ITZ should be in a low temperature and low humidity environment. It is important to note that the two-month physical stability study can only give a preliminary idea of the stability of this system, which can be used to select relatively ideal storage conditions. Longer storage times are required to give more rigorous conclusions about the dosage form stability.

4. Conclusion

The pH-responsive cationic cellulose beads DAC4-EDA were successfully prepared by the modification of EDA onto DAC by Schiff base reaction. In this work, the effect of EDA content on the swelling behavior of DAC-EDA was first investigated, and then the release behavior of three model drugs loaded in DAC-EDA was evaluated, focusing on the effect of bead size and EDA ratio on the release. The results show that IND and ITZ loaded in DAC-EDA lead to an amorphous arrangement, while FNB is partially crystalline in beads prepared with a high ratio of EDA. *In vitro* dissolution testing showed that DAC-EDA improved the apparent solubility and supersaturation of the three model drugs, especially in the case of ITZ, the maximum release percentage from DAC-EDA1-S is 40-fold of that of the crystalline state. The release behavior was influenced by the bead size and EDA content, with small sized beads and high ratio of EDA tending to achieve faster dissolution rates and highest extent. Physical stability experiments showed that the ITZ-loaded DAC-EDA beads remained amorphous for up to two months at three conditions (0 °C/0 %RH, 0 °C/32 %RH and 25 °C/32 %RH), while crystallization occurred in a high temperature and high humidity environment (40 °C/75 %RH) after 2 months storage. In general, DAC4-EDA beads solve the limitations in the drug release of pristine cellulose beads and thus show potential as a carrier for improving the solubility and dissolution rate of poorly water-soluble drugs.

CRediT authorship contribution statement

Fan Xie: Conceptualization, Methodology, Data curation, Formal analysis, Validation, Writing – original draft, Writing – review & editing. **Jernej Slak:** Data curation, Formal analysis. **Pedro Fardim:** Conceptualization, Methodology, Supervision, Writing – review & editing. **Guy Van den Mooter:** Conceptualization, Methodology, Supervision, Writing – review & editing.

Declaration of Competing Interest

The authors declare the following financial interests/personal relationships which may be considered as potential competing interests:

Fan Xie reports financial support was provided by CSC.

Data availability

Data will be made available on request.

Acknowledgements

The authors would like to thank Bernard Appeltans (Drug Delivery and Disposition, KU Leuven) for technical assistance. China Scholarship Council (CSC) and KU Leuven Industrial Research Fund are acknowledged for their support.

Appendix A. Supplementary data

Supplementary data to this article can be found online at https://doi.org/10.1016/j.ijpx.2022.100146.

References

Bhan, C., Verma, L., Singh, J., 2020. Alternative fuels for sustainable development. In: Shukla, V., Kumar, N. (Eds.), Environmental Concerns and Sustainable Development: Volume 1: Air, Water and Energy Resources. Springer, Singapore, pp. 317–331. https://doi.org/10.1007/978-981-13-5889-0_16.

Dang, X., Liu, P., Yang, M., Deng, H., Shan, Z., Zhen, W., 2019. Production and characterization of dialdehyde cellulose through green and sustainable approach. Cellulose 26, 9503–9515. https://doi.org/10.1007/s10570-019-02747-9.

De Wever, P., de Oliveira-Silva, R., Marreiros, J., Ameloot, R., Sakellariou, D., Fardim, P., 2021. Topochemical Engineering of Cellulose—Carboxymethyl Cellulose Beads: A Low-Field NMR Relaxometry Study. Molecules 26 (1), 14. https://doi.org/10.3390/molecules26010014.

Dedroog, S., Boel, E., Kindts, C., Appeltans, B., Van den Mooter, G., 2021. The underestimated contribution of the solvent to the phase behavior of highly drug loaded amorphous solid dispersions. Int. J. Pharm. 609, 121201 https://doi.org/10.1016/j.ijpharm.2021.121201.

Druel, L., Kenkel, A., Baudron, V., Buwalda, S., Budtova, T., 2020. Cellulose aerogel microparticles via emulsion-coagulation technique. Biomacromolecules 21, 1824–1831. https://doi.org/10.1021/acs.biomac.9b01725.

Fink, H.-P., Weigel, P., Purz, H.J., Ganster, J., 2001. Structure formation of regenerated cellulose materials from NMMO-solutions. Prog. Polym. Sci. 26, 1473–1524. https://doi.org/10.1016/S0079-6700(01)00025-9.

Gericke, M., Trygg, J., Fardim, P., 2013. Functional cellulose beads: preparation, characterization, and applications. Chem. Rev. 25.

Jiang, G., Huang, W., Li, L., Wang, X., Pang, F., Zhang, Y., Wang, H., 2012. Structure and properties of regenerated cellulose fibers from different technology processes. Carbohydr. Polym. 87, 2012–2018. https://doi.org/10.1016/j.carbpol.2011.10.022.

Kim, U.-J., Lee, Y.R., Kang, T.H., Choi, J.W., Kimura, S., Wada, M., 2017. Protein adsorption of dialdehyde cellulose-crosslinked chitosan with high amino group contents. Carbohydr. Polym. 163, 34–42. https://doi.org/10.1016/j.carbpol.2017.01.052.

Klemm, D., Heublein, B., Fink, H.-P., Bohn, A., 2005. Cellulose: fascinating biopolymer and sustainable raw material. Angew. Chem. Int. Ed. 44, 3358–3393. https://doi.org/10.1002/anie.200460587.

Liu, S., Du, G., Yang, H., Su, H., Ran, X., Li, J., Zhang, L., Gao, W., Yang, L., 2021. Developing High-Performance Cellulose-based Wood Adhesive with a Cross-Linked Network. ACS Sustain. Chem. Eng. 9, 16849–16861. https://doi.org/10.1021/acssuschemeng.1c07012.

Luo, X., Zhang, L., 2010. Creation of regenerated cellulose microspheres with diameter ranging from micron to millimeter for chromatography applications. J. Chromatogr. A 1217, 5922–5929. https://doi.org/10.1016/j.chroma.2010.07.026.

Malamatari, M., Somavarapu, S., Taylor, K.M.G., Buckton, G., 2016. Solidification of nanosuspensions for the production of solid oral dosage forms and inhalable dry powders. Expert Opin. Drug Deliv. 13, 435–450. https://doi.org/10.1517/17425247.2016.1142524.

Mellaerts, R., Jammaer, J.A.G., Van Speybroeck, M., Chen, H., Humbeeck, J.V., Augustijns, P., Van den Mooter, G., Martens, J.A., 2008. Physical state of poorly water soluble therapeutic molecules loaded into SBA-15 ordered mesoporous silica carriers: a case study with itraconazole and ibuprofen. Langmuir 24, 8651–8659. https://doi.org/10.1021/la801161g.

Orelma, H., Hokkanen, A., Leppänen, I., Kammiovirta, K., Kapulainen, M., Harlin, A., 2020. Optical cellulose fiber made from regenerated cellulose and cellulose acetate for water sensor applications. Cellulose 27, 1543–1553. https://doi.org/10.1007/s10570-019-02882-3.

Pas, T., Vergauwen, B., Van den Mooter, G., 2018. Exploring the feasibility of the use of biopolymers as a carrier in the formulation of amorphous solid dispersions – part I: Gelatin. Int. J. Pharm. 535, 47–58. https://doi.org/10.1016/j.ijpharm.2017.10.050.

Rosenau, T., Potthast, A., Adorjan, I., Hofinger, A., Sixta, H., Firgo, H., Kosma, P., 2002. Cellulose solutions in N-methylmorpholine-N-oxide (NMMO) – degradation processes and stabilizers. Cellulose 9, 283–291. https://doi.org/10.1023/A:1021127423041.

Schuster, G., Lindner, W., 2011. Chocolate HILIC phases: development and characterization of novel saccharide-based stationary phases by applying non-enzymatic browning (Maillard reaction) on amino-modified silica surfaces. Anal. Bioanal. Chem. 400, 2539–2554. https://doi.org/10.1007/s00216-011-4745-5.

Seddiqi, H., Oliaei, E., Honarkar, H., Jin, J., Geonzon, L.C., Bacabac, R.G., Klein-Nulend, J., 2021. Cellulose and its derivatives: towards biomedical applications. Cellulose 28, 1893–1931. https://doi.org/10.1007/s10570-020-03674-w.

Speybroeck, M.V., Barillaro, V., Thi, T.D., Mellaerts, R., Martens, J., Humbeeck, J.V., Vermant, J., Annaert, P., Den Mooter, G.V., Augustijns, P., 2009. Ordered mesoporous silica material SBA-15: a broad-spectrum formulation platform for poorly soluble drugs. J. Pharm. Sci. 98, 2648–2658. https://doi.org/10.1002/jps.21638.

Tipduangta, P., Takieddin, K., Fábián, L., Belton, P., Qi, S., 2015. A new low melting-point polymorph of fenofibrate prepared via talc induced heterogeneous nucleation. Cryst. Growth Des. 15, 5011–5020. https://doi.org/10.1021/acs.cgd.5b00956.

Trygg, J., Fardim, P., Gericke, M., Mäkilä, E., Salonen, J., 2013. Physicochemical Design of the Morphology and Ultrastructure of Cellulose Beads. Carbohydrate Polymers 93 (1), 291–299. https://doi.org/10.1016/j.carbpol.2012.03.085.

Voon, L.K., Pang, S.C., Chin, S.F., 2016. Highly porous cellulose beads of controllable sizes derived from regenerated cellulose of printed paper wastes. Mater. Lett. 164, 264–266. https://doi.org/10.1016/j.matlet.2015.10.161.

Voon, L.K., Pang, S.C., Chin, S.F., 2017. Porous cellulose beads fabricated from regenerated cellulose as potential drug delivery carriers. J. Chemother. 2017, e1943432 https://doi.org/10.1155/2017/1943432.

Vraníková, B., Niederquell, A., Šklubalová, Z., Kuentz, M., 2020. Relevance of the theoretical critical pore radius in mesoporous silica for fast crystallizing drugs. Int. J. Pharm. 591, 120019 https://doi.org/10.1016/j.ijpharm.2020.120019.

Wang, S., Lu, A., Zhang, L., 2016. Recent advances in regenerated cellulose materials. Prog. Polym. Sci. 53, 169–206. https://doi.org/10.1016/j.progpolymsci.2015.07.003.

Xie, F., Fardim, P., Van den Mooter, G., 2022. Porous soluble dialdehyde cellulose beads: a new carrier for the formulation of poorly water-soluble drugs. Int. J. Pharm. 615, 121491 https://doi.org/10.1016/j.ijpharm.2022.121491.

Yildir, E., Kolakovic, R., Genina, N., Trygg, J., Gericke, M., Hanski, L., Ehlers, H., Rantanen, J., Tenho, M., Vuorela, P., Fardim, P., Sandler, N., 2013. Tailored beads made of dissolved cellulose—Investigation of their drug release properties. Int. J. Pharm. 456, 417–423. https://doi.org/10.1016/j.ijpharm.2013.08.047.

Zhang, S., Li, F.-X., Yu, J., Hsieh, Y.-L., 2010. Dissolution behaviour and solubility of cellulose in NaOH complex solution. Carbohydr. Polym. 81, 668–674. https://doi.org/10.1016/j.carbpol.2010.03.029.

Zhou, D., Zhang, L., Zhou, J., Guo, S., 2004. Cellulose/chitin beads for adsorption of heavy metals in aqueous solution. Water Res. 38, 2643–2650. https://doi.org/10.1016/j.watres.2004.03.026.